Energy Transfer Hot Paper

How to cite: *Angew. Chem. Int. Ed.* **2021**, *60*, 19648–19652
International Edition: doi.org/10.1002/anie.202105297
German Edition: doi.org/10.1002/ange.202105297

Enantiospecific Detection of D-Amino Acid through Synergistic Upconversion Energy Transfer

Yongan Tang, Xiaoyan Zhong, Shuangqian Yan, Xiaowang Liu, Liang Cheng, Yu Wang, and Xiaogang Liu**

Abstract: *D-amino acids (DAAs) are indispensable in regulating diverse metabolic pathways. Selective and sensitive detection of DAAs is crucial for understanding the complexity of metabolic processes and managing associated diseases. However, current DAA detection strategies mainly rely on bulky instrumentation or electrochemical probes, limiting their cellular and animal applications. Here we report an enzyme-coupled nanoprobe that can detect enantiospecific DAAs through synergistic energy transfer. This nanoprobe offers near-infrared upconversion capability, a wide dynamic detection range, and a detection limit of 2.2 μM, providing a versatile platform for in vivo noninvasive detection of DAAs with high enantioselectivity. These results potentially allow real-time monitoring of biomolecular handedness in living animals, as well as developing antipsychotic treatment strategies.*

Although L-amino acids have long been considered to have strict homochirality in mammalian tissues,[1] several D-amino acids (DAAs) have recently been found to fulfilled irreplaceable functions in numerous physiological processes of humans.[2] For instance, D-serine (Ser) levels are higher in the hippocampus and parietal cortex of patients with Alzheimer's disease and lower in the serum of patients with schizophrenia than in the controls.[3,4] D-aspartate is essential for synthesizing and secreting several pivotal hormones.[5] Additionally, an elevated D-alanine concentration in gastric juice of carcinoma patients can be considered a potential cancer marker.[6]

Owing to the medicinal importance of DAAs, innovative strategies have been developed for accurate DAA detection.[7] However, most of these strategies rely on complicated instruments. Moreover, they are time- and cost-consuming and infeasible for in vivo detection.[8] DAA oxidase (DAAO) is a highly enantiospecific enzyme that catalyzes DAA oxidation via O_2 consumption along with H_2O_2 production, while non-reactive to its enantiomeric counterparts, namely, L-amino acids, even at high concentrations.[9] Because of the enantiospecific nature of this enzyme, it qualifies for DAA detection, particularly considering the ubiquitous disturbance of chemically similar L-amino acids. DAA detection strategies have been established using DAAO-containing microsensors,[10] microelectrode arrays,[11] or DNA/silver nanoclusters[12] by monitoring the electrochemical or UV-visible spectroscopic signals. However, the limitations of existing probes, such as large physical dimensions, narrow detection range, and limited tissue penetration of UV-visible photons, generally hinder their practical applications (Table S1).

To overcome challenges encountered in DAA detection, we fabricated a near-infrared (NIR)-excitable, enzyme-based nanoprobe that could detect DAAs through synergic upconversion energy transfer (Figure 1). This nanoprobe comprises four components: upconversion nanoparticle (UCNP), platinum porphyrin (PtTFPP), cyanine-dopamine conjugate (CyD), and DAAO. The UCNP can convert NIR light into

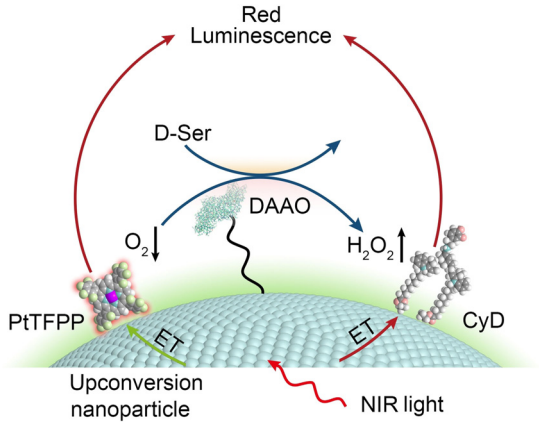

Figure 1. Illustration of enantiospecific enzyme-based nanoprobes for D-Ser detection. Enantiospecific oxidation of D-Ser using DAAO results in O_2 consumption and H_2O_2 production, boosting PtTFPP emission and suppressing CyD absorbance. This dual effect leads to synergistic red luminescence enhancement for D-Ser detection through upconversion energy transfer (ET).

[*] Dr. Y. Tang, Dr. S. Yan, Prof. Y. Wang, Prof. X. Liu
SZU-NUS Collaborative Innovation Center for Optoelectronic Science & Technology, International Collaborative Laboratory of 2D Materials for Optoelectronics Science and Technology of Ministry of Education, Institute of Microscale Optoelectronics
Shenzhen University, Shenzhen 518060 (China)
E-mail: wangyu@szu.edu.cn

Dr. Y. Tang, Dr. S. Yan, Prof. X. Liu
Department of Chemistry, National University of Singapore
Singapore 117549 (Singapore)
E-mail: chmlx@nus.edu.sg

Dr. X. Zhong, Prof. L. Cheng
Institute of Functional Nano & Soft Materials (FUNSOM), Jiangsu Key Laboratory for Carbon-Based Functional Materials and Devices
Soochow University, Suzhou 215123 (China)

Prof. X. Liu
MIIT Key Laboratory of Flexible Electronics (KLoFE) and Xi'an Institute of Flexible Electronics
Northwestern Polytechnical University
710072 Xi'an, Shaanxi (China)

Supporting information and the ORCID identification number(s) for the author(s) of this article can be found under: https://doi.org/10.1002/anie.202105297.

UV/visible photons with minimal background luminescence, offer significant advantages for cellular and animal applications.[13] In the absence of DAAs, PtTFPP and UCNP luminescence was quenched by dissolved O_2 and CyD, respectively. However, in the presence of DAAs, the enantiospecific catalysis by DAAO triggers O_2 depletion and H_2O_2 production, which enhances PtTFPP emission and reduces CyD absorbance, respectively, thereby synergistically boosting red emission intensity. Owing to the large tissue penetration depth of NIR light[14] and stereochemical-specific property of DAAO, these nanoprobes enable sensitive in vivo DAA detection with noninvasive and strict enantiospecific characteristics.

Yb/Er-codoped UCNPs with a well-controlled core–shell-shell structure ($NaYF_4$@$NaYF_4$:Yb/Er (18/2 mol%)@$NaYF_4$) emitted intense green (Er^{3+}: $^2H_{11/2}$, $^4S_{3/2}\rightarrow{}^4I_{15/2}$) and red ($Er^{3+}$: $^4F_{9/2}\rightarrow{}^4I_{15/2}$) light (Figures S1, S2 and Table S2).[15] Amphiphilic polyethylene glycol (PEG) derivatives were used to modify as-synthesized UCNPs and assist PtTFPP, CyD, and DAAO loading (Figure S3).[16] These nanoprobes exhibited a uniform size with pseudospherical morphology (Figure 2A), as well as clear lattice fringes of (110) planes ($d = 0.532$ nm) and a fluffy organic layer with ca. 1.61-nm thickness (Figure S4). Moreover, these PEG-modified nanoprobes showed good water dispersibility and a suitable hydrodynamic dimension (ca. 123.4 nm) for wide detection applications (Figure S4 and Table S3).

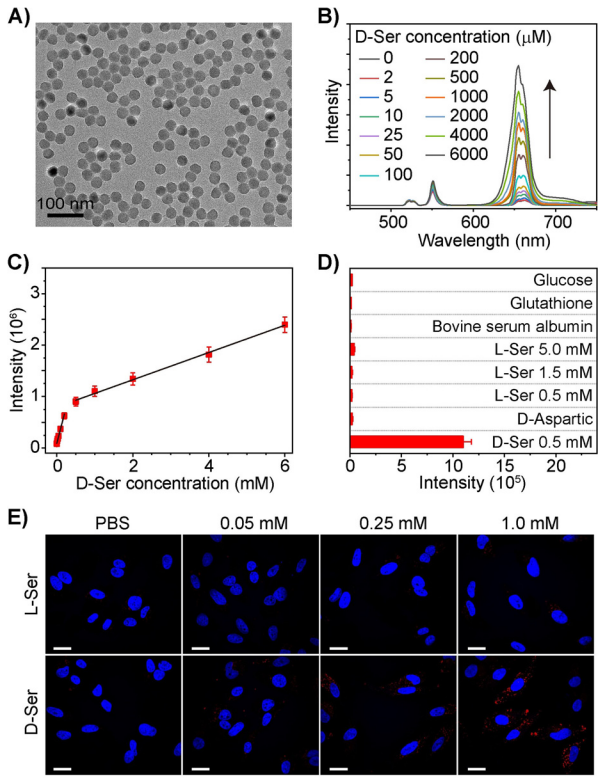

Figure 2. DAA detection in solutions and HeLa cells using the proposed nanoprobes. A) Representative transmission electron microscope image of nanoprobes. B) Emission spectra of a mixture of nanoprobes (3.0 mg mL^{-1}) and D-Ser at various concentrations (Ex., 980 nm). C) Calibration curve for detecting D-Ser. D) Detection selectivity of the nanoprobes. E) Confocal images (Ex., 980 nm, 0.5 W cm^{-2}) of HeLa cells after incubation with nanoprobes (0.5 mg mL^{-1}) for 4 h. Luminescence is collected at 600–670 nm. Scale bar: 20 μm. Data represent mean ± sd.

The DAA detection capability of as-prepared probes was verified by upconversion luminescence of a mixture of nanoprobes and D-Ser under 980-nm laser excitation. The red luminescence band significantly increased when the D-Ser concentration was varied from 0 to 6.0 mM (Figure 2B). The evolution profile can be divided into two phases, which may indicate two sensing signs of progress. Red emission band at 600–670 nm was used to quantify D-Ser concentration (Figure 2C). The minimum detection limit is ca. 2.2 μM with a signal-to-noise ratio of 3, which is encouraging when considering the fact that D-Ser levels in the cerebrospinal fluid of patients with Alzheimer's disease (12.32 μM) are significantly elevated than the control (2.45 μM).[3] We further measured the relative contribution of CyD and PtTFPP to detected signals as well as detection kinetics (Figures S5 and S6). Additionally, our nanoprobes exhibited high enantiospecific selectivity. At considerably high concentrations (3 and 10 times), L-Ser as well as common biological molecules, including bovine serum albumin, glutathione, and glucose, did not produce significant signal (Figure 2D). It is worth noting that our nanoprobes also exhibit high selectivity for D-Ser against other DAAs such as D-aspartate, owing to the intrinsic selectivity of DAAO. Moreover, the acceptable coefficient of variation (5.9–10.5%), analytical recovery (90.5–112.3%), and batch-to-batch reproducibility of our nanoprobes were confirmed (Table S4 and Figure S7).

We next monitored intracellular D-Ser levels on HeLa cells. After 4 h of incubation, red emission remained conspicuous even at a high L-Ser concentration (1.0 mM). Conversely, the red emission brightened at a low D-Ser concentration (0.05 mM, Figure 2E). Further, at D-Ser concentrations of 0.25 and 1.0 mM, luminescence intensity improved by approximately 6- and 12-folds, respectively (Figure S5), strongly indicating the feasibility and specificity of the nanoprobes for monitoring intracellular DAAs.

A comparison of our approach with existing DAA detection strategies shows advantages of our work (Table S1), including both excitation and emission in the NIR window, nanoscale dimension, a wide detection range, and a low detection limit, as well as a cellular detection capability. The outstanding performance of the nanoprobes under investigation was attributed to the on-demand material design and precise engineering control. In nearly all previous DAAO-based detection strategies, DAA was enantiospecifically quantified by solely sensing the O_2 or H_2O_2 level variation triggered by catalytic reactions (Table S1), leading to high noise and limited response range owing to disturbances from O_2 and H_2O_2. However, our nanoprobes exhibited dual-sensing capabilities for H_2O_2 production and O_2 consumption (Figure 3A), indicating successful integration of these two sensing principles (Figure S8). Additionally, the two sensing principles lead to red-emission amplification, which is favorable due to its convenience and simplicity. This amplification is enabled by manipulating synergistic energy transfer from UCNPs to CyD and PtTFPP.

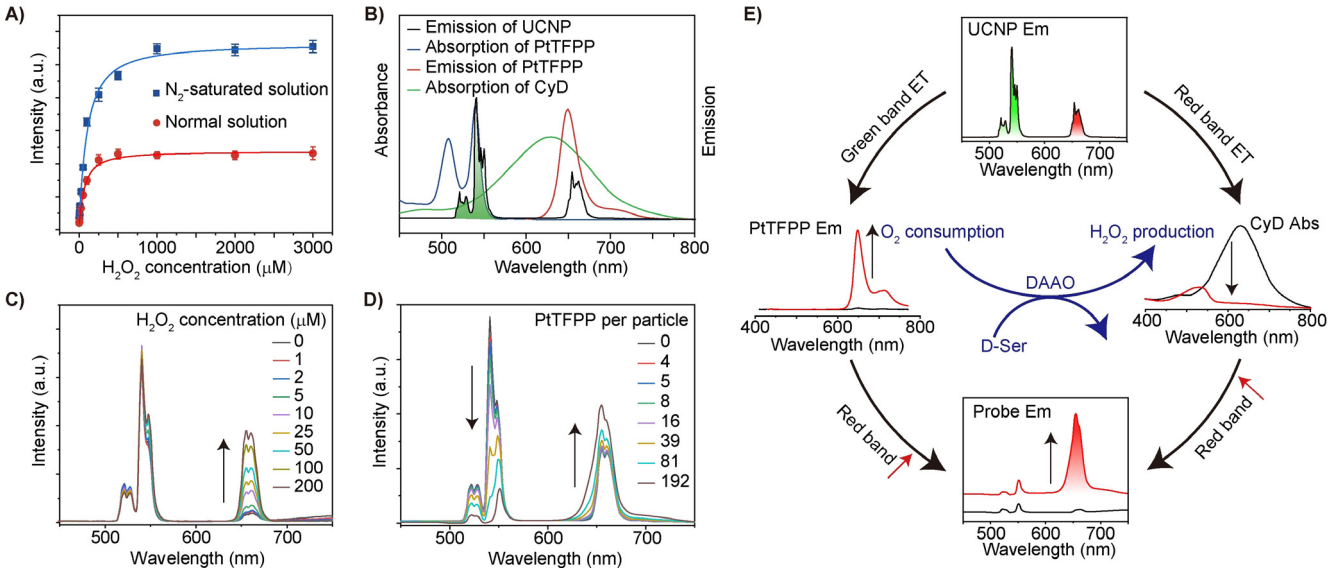

Figure 3. Dual sensing of O_2 & H_2O_2 and synergistic upconversion energy transfer. A) Upconversion luminescence intensity of the nanoprobes in a normal or N_2-saturated solution with varying H_2O_2 concentrations. B) Upconversion emission spectrum of UCNPs, absorption and emission spectra of PtTFPP (Ex. = 540 nm), and absorption spectrum of CyD. C) Emission spectra of CyD-loaded UCNPs in normal solutions with varying H_2O_2 concentrations. D) Emission spectra of PtTFPP-loaded UCNPs with varying PtTFPP-loading numbers in N_2-saturated solutions. E) Dual-sensing of O_2 & H_2O_2 and synergistic upconversion energy transfer. Abbreviation: ET, energy transfer; Em, emission; and Abs, absorption. A 980-nm laser is used as the light source.

Energy transfer from UCNPs to CyD and PtTFPP was investigated using two control probes, CyD-loaded and PtTFPP-loaded UCNPs, respectively, to diminish the mutual interference. In CyD-loaded UCNPs, CyD was used as the energy acceptor. The absorption spectrum of CyD well matches the red band (640–680 nm, Er^{3+}, $^4F_{9/2} \rightarrow {}^4I_{15/2}$) of UCNPs (Figure 3B), indicating potential energy transfer manipulation.[17] The efficient energy transfer between them was proved by the results that the UCNP luminescence, particularly the red emission, was significantly quenched through CyD loading (Figure S9). Moreover, CyD exhibited a sharp reduction in red absorption (550–750 nm) in the presence of H_2O_2 (Figure S9),[18] which could relieve luminescence quenching. Consequently, red luminescence from UCNPs recovered with increasing H_2O_2 concentration, suggesting that H_2O_2 can be sensed by 980-nm excited red luminescence through energy transfer (Figure 3C).

In PtTFPP-loaded UCNPs, PtTFPP was used as the energy acceptor for O_2 consumption sensing.[19] The emission intensities of free PtTFPP and PtTFPP-loaded UCNPs in nitrogen-saturated solutions increased by approximately 2.2- and 6.2-fold, respectively, compared with those in normal solutions (Figure S10), strongly suggesting that the nanoprobes were more sensitive to O_2 consumption than free dyes.[20] The luminescence quantum yield of PtTFPP-loaded UCNPs was higher than that of free PtTFPP in nitrogen-saturated solutions, further confirming the improved O_2 sensitivity (Figure S10).[21] Moreover, the overlap of the PtTFPP absorption and green band (510–560 nm, $^2H_{11/2}$, $^4S_{3/2} \rightarrow {}^4I_{15/2}$) of UCNPs suggested possible energy transfer (Figure 3B),[22] which was investigated by increasing the PtTFPP loading numbers (Figure S10). Under 980-nm excitation, we recorded a strong quenching of the characteristic green emission from UCNPs in favor of the red PtTFPP emission at 625–750 nm in nitrogen-saturated solutions (Figure 3D). These findings verified efficient energy transfer between these two primary components, as further confirmed by the decrease in the lifetime (540 nm, $^4S_{3/2} \rightarrow {}^4I_{15/2}$ transition of Er^{3+}) from 96.1 μs without PtTFPP to 52.9 μs with ca. 192 PtTFPP molecules per particle (Figure S10 and Table S5).[23] However, in sharp contrast, the enhanced red PtTFPP emission was barely observed in normal solution (Figure S10), suggesting that O_2 consumption can be sensed using 980-nm excited red luminescence through energy transfer. Core-shell-shell UCNPs were designed to maximize energy transfer efficiency (Figures S11 and S12). Particularly, the PtTFPP emission (625–750 nm) well matched the red UCNP band and CyD absorption, which was purposely used to construct a synergistic energy transfer system.

The O_2 and H_2O_2 dual sensing and synergistic upconversion energy transfer in nanoprobes are illustrated in Figure 3E. The energies of the green and red bands of UCNPs were accepted by PtTFPP and CyD, respectively. With D-Ser oxidation, O_2 consumption and H_2O_2 production induced enhanced PtTFPP emission and reduced CyD red absorbance, yielding a synergistic red luminescence (600–750 nm) enhancement for high-sensitive DAA detection with both excitation and emission in the NIR range.

Interestingly, the as-synthesized nanoprobes proved effective for in vivo noninvasive DAA detection. These nanoprobes were subcutaneously injected into the back of the mice, followed by intraperitoneal injection of D/L-Ser. The probe injection site rapidly brightened 15 min after the D-Ser injection, and the intensity reached its peak 30 min after the injection (Figure 4A). Compared with that before the D-Ser injection, the maximum luminescence intensity increased

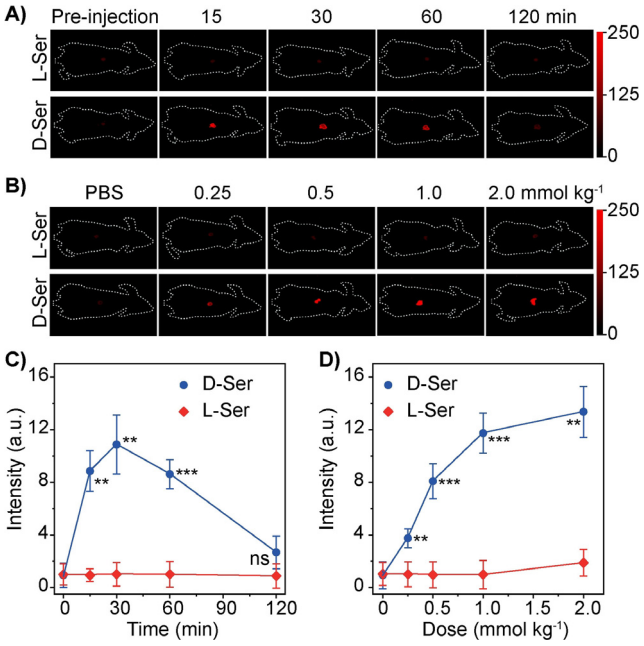

Figure 4. In vivo DAA detection (Ex., 980 nm, 0.5 $W cm^{-2}$) by subcutaneously injecting nanoprobes (10.0 $mg kg^{-1}$) into the back of the mice, followed by intraperitoneal injection of 100-μL D/L-Ser. Upconversion luminescence images of the nude mice and corresponding signal intensities acquired 120 min after D/L-Ser injection at a dose of 1.0 $mmol kg^{-1}$ (A and C), or acquired 30 min after D/L-Ser injection at varying doses (B and D). $n = 3$. $^{**}p < 0.01$, $^{***}p < 0.001$, and ns denotes not significant ($p > 0.05$), analyzed using Student's t-test. Data represent mean ± sd.

about 11 times (Figure 4C), indicating the nanoprobes' sensitive response to D-Ser in vivo. In contrast, L-Ser injection induced no marked changes in imaging and emission intensity, further indicating the strict stereoselectivity of the nanoprobes. Finally, the response of nanoprobes to D/L-Ser under various doses was further investigated. Upconversion luminescence signals were positively related to D-Ser doses in both imaging and emission intensity (Figure 4B,D). L-Ser did not trigger any significant fluorescence at high doses. In addition, we have preliminarily assessed nanoprobe toxicity using hematoxylin-eosin staining and serum biochemistry assay (Figure S13).

In summary, we have proposed NIR light-excited nanoprobes for DAA detection through synergistic upconversion energy transfer. These nanoprobes exhibit desirable luminescence properties, such as both excitation and emission in the NIR range, small dimension, a wide detection range, a low detection limit, and a dual-sensing capability. By leveraging the deep tissue penetration of NIR light and the high stereochemical specificity of the nanoprobes, D-Ser levels in living cells and mice can be conveniently monitored with high sensitivity and selectivity, enabling noninvasive detection with time- and cost-saving. To the best of our knowledge, this is the first study focusing on UCNPs for chiral molecular detection. We envision that these nanoprobes will find critical applications in brain-related biological and medical research, particularly when considering essential physiological roles of DAAs and other chiral components,[24] as well as advantageous optical properties of UCNPs.[25]

Acknowledgements

The authors acknowledge the support from National Natural Science Foundation of China (grant 61805153, 61705137, 21775049), the Science and Technology Project of Shenzhen (grant JCYJ20170817093821657, KQJSCX20180328093614762), China Postdoctoral Science Foundation (2018M643174), Singapore Ministry of Education (MOE2017-T2-2-110), and National Research Foundation, the Prime Minister's Office of Singapore under its NRF Competitive Research Programme (Award No. NRF-CRP23-2019-0070).

Conflict of Interest

The authors declare no conflict of interest.

Keywords: chiral detection · D-amino acid · energy transfer · lanthanide-doped nanoparticles · near-infrared light

[1] a) F. Y. Thanzeel, C. Wolf, *Angew. Chem. Int. Ed.* **2017**, *56*, 7276 – 7281; *Angew. Chem.* **2017**, *129*, 7382 – 7387; b) R. Breslow, Z.-L. Cheng, *Proc. Natl. Acad. Sci. USA* **2009**, *106*, 9144 – 9146.
[2] a) S. Beltrán-Castillo, M. J. Olivares, R. A. Contreras, G. Zúñiga, I. Llona, R. von Bernhardi, J. L. Eugenín, *Nat. Commun.* **2017**, *8*, 838; b) X. Dai, E. Zhou, W. Yang, X. Zhang, W. Zhang, Y. Rao, *Nat. Commun.* **2019**, *10*, 1986; c) C. Ridler, *Nat. Rev. Gastroenterol. Hepatol.* **2016**, *13*, 499; d) J. Sasabe, Y. Miyoshi, M. Suzuki, M. Mita, R. Konno, M. Matsuoka, K. Hamase, S. Aiso, *Proc. Natl. Acad. Sci. USA* **2012**, *109*, 627 – 632; e) Z. Cheng, E. Kuru, A. Sachdeva, M. Vendrell, *Nat. Rev. Chem.* **2020**, *4*, 275 – 290; f) Y. Li, C. Liu, X. Bai, F. Tian, G. Hu, J. Sun, *Angew. Chem. Int. Ed.* **2020**, *59*, 3486 – 3490; *Angew. Chem.* **2020**, *132*, 3514 – 3518; g) A. J. Boersma, H. Bayley, *Angew. Chem. Int. Ed.* **2012**, *51*, 9606 – 9609; *Angew. Chem.* **2012**, *124*, 9744 – 9747.
[3] C. Madeira, M. V. Lourenco, C. Vargas-Lopes, C. K. Suemoto, C. O. Brandão, T. Reis, R. E. P. Leite, J. Laks, W. Jacob-Filho, C. A. Pasqualucci, L. T. Grinberg, S. T. Ferreira, R. Panizzutti, *Transl. Psychiatry* **2015**, *5*, e561.
[4] N. El-Tallawy, T. H. Saleem, A. M. El-Ebidi, M. H. Hassan, R. H. Gabra, W. M. Farghaly, N. A. El-Maali, H. S. Sherkawy, *Neuropsychiatr. Dis. Treat.* **2017**, *13*, 1057 – 1063.
[5] G. Genchi, *Amino Acids* **2017**, *49*, 1521 – 1533.
[6] Y. Nagata, T. Sato, N. Enomoto, Y. Ishii, K. Sasaki, T. Yamada, *Amino Acids* **2007**, *32*, 137 – 140.
[7] a) Y. Zeng, P. Qi, D. Zhang, *Anal. Methods* **2020**, *12*, 3404 – 3410; b) Y. Wang, X. Q. Zhao, Z. Yu, Z. R. Xu, B. Zhao, Y. Ozaki, *Angew. Chem. Int. Ed.* **2020**, *59*, 19079 – 19086; *Angew. Chem.* **2020**, *132*, 19241 – 19248; c) H. Yuan, Y. Huang, J. Yang, Y. Guo, X. Zeng, S. Zhou, J. Cheng, Y. Zhang, *Spectrochim. Acta Part A* **2018**, *200*, 330 – 338; d) L. Pu, *Angew. Chem. Int. Ed.* **2020**, *59*, 21814 – 21828; *Angew. Chem.* **2020**, *132*, 21998 – 22012.
[8] a) C. S. Pundir, S. Lata, V. Narwal, *Biosens. Bioelectron.* **2018**, *117*, 373 – 384; b) G. Molla, L. Piubelli, F. Volontè, M. S. Pilone, in *Unnatural Amino Acids: Methods and Protocols, Vol. 794* (Eds.: L. Pollegioni, S. Servi), Humana Press, Totowa, NJ, **2012**, pp. 273 – 289.

[9] a) S. Sacchi, L. Caldinelli, P. Cappelletti, L. Pollegioni, G. Molla, *Amino Acids* **2012**, *43*, 1833 – 1850; b) S. V. Khoronenkova, V. I. Tishkov, *Biochemistry* **2008**, *73*, 1511 – 1518.
[10] a) P. Pernot, J.-P. Mothet, O. Schuvailo, A. Soldatkin, L. Pollegioni, M. Pilone, M.-T. Adeline, R. Cespuglio, S. Marinesco, *Anal. Chem.* **2008**, *80*, 1589 – 1597; b) D. Polcari, A. Kwan, M. R. Van Horn, L. Danis, L. Pollegioni, E. S. Ruthazer, J. Mauzeroll, *Anal. Chem.* **2014**, *86*, 3501 – 3507; c) Z. M. Zain, R. D. O'Neill, J. P. Lowry, K. W. Pierce, M. Tricklebank, A. Dewa, S. A. Ghani, *Biosens. Bioelectron.* **2010**, *25*, 1454 – 1459.
[11] D. Campos-Beltrán, Å. Konradsson-Geuken, E. J. Quintero, L. Marshall, *Biosensors* **2018**, *8*, 20.
[12] Z. Zhang, Y. Liu, P. Liu, L. Yang, X. Jiang, D. Luo, D. Yang, *Nanoscale* **2017**, *9*, 19367 – 19373.
[13] a) D. Yang, P. Ma, Z. Hou, Z. Cheng, C. Li, J. Lin, *Chem. Soc. Rev.* **2015**, *44*, 1416 – 1448; b) X. Qiu, Q. Zhou, X. Zhu, Z. Wu, W. Feng, F. Li, *Nat. Commun.* **2020**, *11*, 4; c) S. Xie, Y. Du, Y. Zhang, Z. Wang, D. Zhang, L. He, L. Qiu, J. Jiang, W. Tan, *Nat. Commun.* **2020**, *11*, 1347; d) H. Li, M. Tan, X. Wang, F. Li, Y. Zhang, L. Zhao, C. Yang, G. Chen, *J. Am. Chem. Soc.* **2020**, *142*, 2023 – 2030; e) Z. Yang, K. Y. Loh, Y.-T. Chu, R. Feng, N. S. R. Satyavolu, M. Xiong, S. M. Nakamata Huynh, K. Hwang, L. Li, H. Xing, X. Zhang, Y. R. Chemla, M. Gruebele, Y. Lu, *J. Am. Chem. Soc.* **2018**, *140*, 17656 – 17665; f) Y. Jiang, P. Fu, Y. Liu, C. Wang, P. Zhao, X. Chu, X. Jiang, W. Yang, Y. Wu, Y. Wang, G. Xu, J. Hu, W. Bu, *Sci. Adv.* **2020**, *6*, eabc3513; g) X. Zhang, W. Chen, X. Xie, Y. Li, D. Chen, Z. Chao, C. Liu, H. Ma, Y. Liu, H. Ju, *Angew. Chem. Int. Ed.* **2019**, *58*, 12117 – 12122; *Angew. Chem.* **2019**, *131*, 12245 – 12250.
[14] a) G. Hong, A. L. Antaris, H. Dai, *Nat. Biomed. Eng.* **2017**, *1*, 0010; b) Y. Shao, J. Zhao, J. Yuan, Y. Zhao, L. Li, *Angew. Chem. Int. Ed.* **2021**, *60*, 8923 – 8931; *Angew. Chem.* **2021**, *133*, 9005 – 9013; c) R. Song, H. Wang, M. Zhang, Y. Liu, X. Meng, S. Zhai, C.-c. Wang, T. Gong, Y. Wu, X. Jiang, W. Bu, *Angew. Chem. Int. Ed.* **2020**, *59*, 21032 – 21040; *Angew. Chem.* **2020**, *132*, 21218 – 21226.
[15] W. Zheng, P. Huang, D. Tu, E. Ma, H. Zhu, X. Chen, *Chem. Soc. Rev.* **2015**, *44*, 1379 – 1415.
[16] A. Sedlmeier, H. H. Gorris, *Chem. Soc. Rev.* **2015**, *44*, 1526 – 1560.
[17] a) J. Zhou, C. Li, D. Li, X. Liu, Z. Mu, W. Gao, J. Qiu, R. Deng, *Nat. Commun.* **2020**, *11*, 4297; b) Y. Wu, D. Li, F. Zhou, H. Liang, Y. Liu, W. Hou, Q. Yuan, X. Zhang, W. Tan, *Chem. Sci.* **2018**, *9*, 5427 – 5434; c) Y. Liu, Y. Yang, Y. Sun, J. Song, N. G. Rudawski, X. Chen, W. Tan, *J. Am. Chem. Soc.* **2019**, *141*, 7407 – 7413; d) C. Siefe, R. D. Mehlenbacher, C. S. Peng, Y. Zhang, S. Fischer, A. Lay, C. A. McLellan, A. P. Alivisatos, S. Chu, J. A. Dionne, *J. Am. Chem. Soc.* **2019**, *141*, 16997 – 17005; e) N. Wang, X. Yu, K. Zhang, C. A. Mirkin, J. Li, *J. Am. Chem. Soc.* **2017**, *139*, 12354 – 12357; f) H. Chu, J. Zhao, Y. Mi, Y. Zhao, L. Li, *Angew. Chem. Int. Ed.* **2019**, *58*, 14877 – 14881; *Angew. Chem.* **2019**, *131*, 15019 – 15023; g) J. Li, S. K. Cushing, F. Meng, T. R. Senty, A. D. Bristow, N. Wu, *Nat. Photonics* **2015**, *9*, 601 – 607.
[18] F. Yu, P. Li, P. Song, B. Wang, J. Zhao, K. Han, *Chem. Commun.* **2012**, *48*, 4980 – 4982.
[19] S. Han, R. Deng, Q. Gu, L. Ni, U. Huynh, J. Zhang, Z. Yi, B. Zhao, H. Tamura, A. Pershin, H. Xu, Z. Huang, S. Ahmad, M. Abdi-Jalebi, A. Sadhanala, M. L. Tang, A. Bakulin, D. Beljonne, X. Liu, A. Rao, *Nature* **2020**, *587*, 594 – 599.
[20] R. I. Dmitriev, S. M. Borisov, H. Düssmann, S. Sun, B. J. Müller, J. Prehn, V. P. Baklaushev, I. Klimant, D. B. Papkovsky, *ACS Nano* **2015**, *9*, 5275 – 5288.
[21] Q. Zhao, T. Pan, G. Xiang, Z. Mei, J. Jiang, G. Li, X. Zou, M. Chen, D. Sun, S. Jiang, Y. Tian, *Sens. Actuators B* **2018**, *273*, 242 – 252.
[22] a) N. Hildebrandt, C. M. Spillmann, W. R. Algar, T. Pons, M. H. Stewart, E. Oh, K. Susumu, S. A. Díaz, J. B. Delehanty, I. L. Medintz, *Chem. Rev.* **2017**, *117*, 536 – 711; b) E. R. H. Walter, Y. Ge, J. C. Mason, J. J. Boyle, N. J. Long, *J. Am. Chem. Soc.* **2021**, *143*, 6460 – 6469.
[23] a) Q. Su, W. Feng, D. Yang, F. Li, *Acc. Chem. Res.* **2017**, *50*, 32 – 40; b) M. Dagher, M. Kleinman, A. Ng, D. Juncker, *Nat. Nanotechnol.* **2018**, *13*, 925 – 932; c) Z. Li, S. Lv, Y. Wang, S. Chen, Z. Liu, *J. Am. Chem. Soc.* **2015**, *137*, 3421 – 3427.
[24] a) S. Li, M. Sun, C. Hao, A. Qu, X. Wu, L. Xu, C. Xu, H. Kuang, *Angew. Chem. Int. Ed.* **2020**, *59*, 13915 – 13922; *Angew. Chem.* **2020**, *132*, 14019 – 14026; b) A. Qu, M. Sun, J.-Y. Kim, L. Xu, C. Hao, W. Ma, X. Wu, X. Liu, H. Kuang, N. A. Kotov, C. Xu, *Nat. Biomed. Eng.* **2021**, *5*, 103 – 113; c) H.-E. Lee, H.-Y. Ahn, J. Mun, Y. Y. Lee, M. Kim, N. H. Cho, K. Chang, W. S. Kim, J. Rho, K. T. Nam, *Nature* **2018**, *556*, 360 – 365; d) R. Gao, L. Xu, C. Hao, C. Xu, H. Kuang, *Angew. Chem. Int. Ed.* **2019**, *58*, 3913 – 3917; *Angew. Chem.* **2019**, *131*, 3953 – 3957.
[25] a) Y. Wang, K. Zheng, S. Song, D. Fan, H. Zhang, X. Liu, *Chem. Soc. Rev.* **2018**, *47*, 6473 – 6485; b) S. Chen, A. Z. Weitemier, X. Zeng, L. He, X. Wang, Y. Tao, A. J. Y. Huang, Y. Hashimotodani, M. Kano, H. Iwasaki, L. K. Parajuli, S. Okabe, D. B. L. Teh, A. H. All, I. Tsutsui-Kimura, K. F. Tanaka, X. Liu, T. J. McHugh, *Science* **2018**, *359*, 679 – 684.

Manuscript received: April 18, 2021
Revised manuscript received: June 20, 2021
Accepted manuscript online: July 5, 2021
Version of record online: July 29, 2021

